Bioactive Materials 5 (2020) 798–807

Contents lists available at ScienceDirect

Bioactive Materials

journal homepage: http://www.keaipublishing.com/biomat

3D printing preview for stereo-lithography based on photopolymerization kinetic models

Yi Gao[a,b,1], Lei Xu[c,1], Yang Zhao[a], Zhengwei You[a], Qingbao Guan[a,*]

[a] State Key Laboratory for Modification of Chemical Fibers and Polymer Materials, Shanghai Belt and Road Joint Laboratory of Advanced Fiber and Low-dimension Materials (Donghua University), College of Materials Science and Engineering, Donghua University, Shanghai, 201620, PR China
[b] Center for Combustion Energy and Key Laboratory for Thermal Science and Power Engineering of MOE, Tsinghua University, Beijing, 100084, China
[c] Institute of Agricultural Facilities and Equipment, Jiangsu Academy of Agricultural Sciences, Key Laboratory for Protected Agricultural Engineering in the Middle and Lower Reaches of Yangtze River, Ministry of Agriculture and Rural Affairs, Nanjing, 210014, PR China

ARTICLE INFO

Keywords:
3D printing preview
Photopolymerization kinetics
Biomedical applications
Dental materials
Epoxy acrylate

ABSTRACT

The diversity of biomedical applications makes stereolithographic (SL) three-dimensional (3D) printing process complex. A strategy was developed to simulate the layer-by-layer fabrication of 3D printed products combining polymerization kinetic with reaction conditions to realize print preview. As a representative example, the typical UV-curable dental materials based on epoxy acrylate and photoinitiator with different molar ratios was exposed under varying intensity of UV light to verify the simulation results. A theoretical kinetics model containing oxygen inhibition was established. In-situ FTIR was employed to measure propagation and termination constants while coupled UV/vis was performed to examine the law of light attenuation during cure reaction, even with various colours and additives. Simulation results showed that the correlation coefficient square between the experiments and simulations of epoxy acrylate with 1%, 2% and 3% initiator upon 20 mW/cm^2 UV light are 0.8959, 0.9324 and 0.9337, respectively. Consequently, our simulation of photopolymerization for SL 3D printing successfully realized visualization of printing quality before practically printing the targeted biomedical objects with complex topology structures.

1. Introduction

Biomedical applications for additive manufacturing are one of the current growth leaders within a technology that overall is growing remarkably fast. We are already beginning to experience the integration of additive manufacturing in tissue engineering, dental offices and laboratories. The opportunities for use of polymer-based additive manufactured materials across all aspects of dentistry are widespread but will depend on further improvements in the processing technologies, for instance, a new level of control over the quality and speed of the printing process [1–3]. Compared to the other additive manufacturing technologies such as selective laser sintering, fused deposition modelling and laminated object manufacturing, the unique photo-induced polymerization only in irradiated areas of stereolithographic (SL) 3D printing realizes fabrication of high-resolution structure [4]. The application of photo-polymerization has significantly developed in SL which can manufacture structure with various geometries and scales by layer-by-layer approach [5]. However, a significant challenge regarding SL is the anisotropic bulk mechanical properties in the direction of the axis of printing when using acrylate-based resin as dental materials [6] and the stair casing effect on curved or angled surfaces [7]. This effect can be countered by reduction of the slice thickness in the 2D rendering and implemented by either finely slicing the part throughout or using a technique called adaptive slicing, which enables a user to select regions for thinner slicing [8]. These methods, however, result in a significantly increased build time given the number of mechanical resin renewal steps between each layer exposure. Therefore, the layer-by-layer approach has an intrinsic trade-off between part quality and part build time. It can be concluded that the primary cause for the limitation of the SL platform within the field of rapid manufacturing can be attributed to the layer-by-layer approach.

Recent development of the SL 3D printing technique such as the continuous liquid interface production (CLIP) addresses some of the outlined limitations by achieving new benchmarks in the speed of the

Peer review under responsibility of KeAi Communications Co., Ltd.
* Corresponding author.
E-mail address: qbguan@dhu.edu.cn (Q. Guan).
[1] These authors contributed equally to this work.

https://doi.org/10.1016/j.bioactmat.2020.05.006
Received 20 April 2020; Received in revised form 19 May 2020; Accepted 29 May 2020

printing process without sacrificing its accuracy [9]. The CLIP method takes advantage of the oxygen inhibition [10] of the free radical polymerization in photo-polymerising UV-curable resins, which maintains a layer of liquid at the bottom of the resin container during the polymerization via oxygen-permeable membrane, and this liquid layer (named “dead zone”) is crucial for a continuous supply of the precursor resins to a curing region [11]. Although the formation of the dead zone is kinetically driven, the parameter optimization of light intensity, build speed, and weight percent UV absorber was necessary. The cure thickness of the resin was calculated under static conditions using methods outlined to yield initial fabrication parameters [12]. However, because the CLIP process is dynamic, adjustments are necessary to properly maintain the dead zone throughout the fabrication process. Apparently, the parameter optimizing process is extremely time-consuming and labour-intensive, and it is easy to cause waste of materials. Although the UV cure kinetics of cross-linked polymers with varying thickness have been extensively studied experimentally and theoretically based on differing light intensities and initiator concentrations [13–15], there are few reports on combining the layer-to-layer mechanism with UV cure kinetics to describe the process of SL 3D printing. Compared to the traditional editing and printing software such as OFFICE series with built-in print preview function, additive manufacturing technique, in particular SL 3D printing involving photo-polymerization needs the print preview function to be introduced into the 3D printing software. Herein, we demonstrated that the simulation approach to 3D printing preview function based on general materials and SL apparatus. It allows users to preview the print results and adjust the printer settings in a targeted manner. On the other hand, it automatically designs and recommends printer setting schemes for the imported graphics of different photosensitive resin, in order to reduce the consumables for users to obtain targeting 3D printed products.

2. Materials and methods

2.1. Materials

Bisphenol-A epoxy resin E−51 (Nantong Xingchen Synthetic Material Co. Ltd), acrylate (Sinopharm Chemical Reagent Co. Ltd, CR), 4-methoxypheno (inhibitors, Shanghai Yuanye Bio-Technology Co. Ltd, 98%), tetramethylammonium chloride (catalyst, Sinopharm Chemical Reagent Co. Ltd, AR), triethylene glycol dimethacrylate (TEGDMA, diluent to adjust viscosity, Aladdin, 95%), and 2,4,6-trimethyl benzoyl diphenyl phosphine oxide (TPO, photoinitiator, Shanghai Dibo Bio-Technology Co. Ltd, 98%) were used as received without further purification.

2.2. Synthesis of epoxy acrylate (EA) precursor

35.6 g E−51 and 0.036 g 4-methoxyphenol were added in a 250 mL three-necked round bottom flask with a magnetic stirrer under a steady flow of nitrogen at 70 °C for 10 min until homogenous mixture obtained. Then 0.3539 g tetramethylammonium chloride dissolved completely in 13.16 mL acrylate was added dropwisely to the homogenous mixture in 20 min. The reaction temperature was then increased to 95 °C and isothermally held for 80 min 30 mL TEGDMA was then added in the flask and the reaction was continued stirring at 90 °C for 10 min to get the epoxy acrylate (EA) precursor with moderate viscosity.

2.3. Characterization

The EA sample was sandwiched between two Φ 25 mm × 4 mm KBr crystals using a d8 × 1 mm polymethyl methacrylate (PMMA) ring spacer and exposed simultaneously to the UV beam that induced photopolymerization with the infrared beam (NICOLET 5700, Nicolet Instrument Co. America) monitoring the absorption characteristic peaks of the functional groups. The peak at 1628 cm^{-1} (A_{1628}) referring to the C═C stretching of the vinyl group was chosen as characteristic peak while 1590 cm^{-1} (A_{1590}) assigned to aromatic C═C bond was chosen as internal standard one and two ends of base line were fixed at 1656 cm^{-1} and 1546 cm^{-1}. The degree of conversion (x) at any time (t) was then calculated by internal standard method as follows:

$$x = \frac{\frac{A_{1628}(0)}{A_{1590}} - \frac{A_{1628}(t)}{A_{1590}}}{\frac{A_{1628}(0)}{A_{1590}}} \times 100\% \quad (1)$$

Ultraviolet/visible spectroscopy (UV/vis) was used to measure light absorbance of 365 nm in EA precursor, TPO and EA resins to detect how the light intensity changing with the polymerization. Various concentrations of TPO, precursor diluted with chloroform and different depths of EA resins were prepared for measurement.

The themo-dilatometric responses of EA with different concentration of PI (1 wt%, 2 wt% and 3 wt%) after being exposed to 40 mw/cm^2 UV light for 90 s were measured using a thermomechanical analyzer (TMA, Q400, TA, USA) from 25 °C to 150 °C at a ramp rate of 5 °C/min. The CTE of EA monomer (CTE_m) was measured by a dilatometer which was similar to thermometer in principle and calculated as following:

$$CTE_m = \frac{\pi D^2/4}{V_0} \times k \quad (2)$$

where D is the inner diameter of capillary, V_0 is original liquid volume, k is the slope of the linear fitting applied to temperature and dimension change EA monomer.

The T_g values of EA before and after curing were determined using a differential scanning calorimeter (DSC, Q200, TA, USA) at a ramp rate of 20 °C/min and were calculated as the mid-point between the pre- and post-transition baselines in the thermogram.

3. Results

3.1. Parameter determination and analysis

SL that creates parts by laser-curing successive layers of liquid resin [16], of which the layer thickness (25–200 μm) is sliced according to the predetermined structure using layer-by-layer fabrication process as shown in Fig. 1A. The resin in the container is cured by a digital light projector in a defined thickness and time (2–10 s). The support layer is cured in relatively more time to ensure good adherence support platform. The body structures are then built bottom-up as the support platform arising. In the case of some products with complex topology structure where each layer needs considerably different content of resin, post-curing with UV light is highly required as the conversion of functional groups is incomplete which may affect the mechanical properties of products. Fig. 1B shows the polymer network formation driven by UV radical photopolymerization, and its kinetic model is summarized in Table S1. Polymer chains containing pendant bonds are firstly formed from monomer initiated by photoinitiator (PI) and further propagation can proceed by addition of next monomer. Eventually, the polymer chains can form a crosslinked network through both intramolecular and intermolecular reactions [17]. With the oxygen atmosphere, inhibition will take place which may quench the excited state of PI and then react with primary initiating or propagating radicals to form peroxyl radical to terminate polymerization [18], leading to more complex reaction-diffusion models. Herein, the typical dental resin epoxy acrylate (EA) precursor designed for kinetics simulations has been synthesized from a polycondensation reaction (Fig. 1C) with relatively clear understanding of EA structure and easy control of its constituents [19]. The physical properties of EA precursor resin are summarized in Table S2 and its structure and in-situ photopolymerization was investigated using real-time UV light-FTIR spectra.

It is well known that higher reaction rates and crosslinking density stemming from higher degree functionality. Though the monomers with shorter chains have higher final conversion, the network

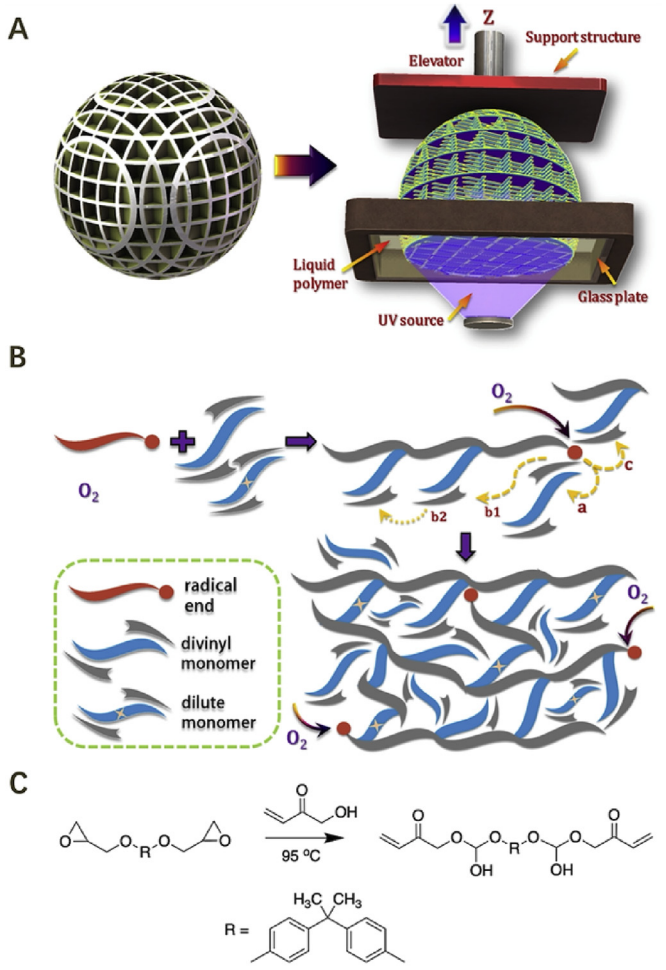

Fig. 1. Illustration of the SL 3D printer and photopolymerization mechanism. (A) Schematic of the SL 3D printer. (B) Schematic mechanism of UV radical photopolymerization with oxygen inhibition. (C) Synthetic route for the typical dental resin EA precursor.

inhomogeneity is higher [20,21]. The consumption of functional groups or production of polymer is evaluated to quantify the reaction process. Decker et al. [18] developed the pioneering utilization of real-time FTIR to monitor the concentration of C=C bonds consuming with the photoinduced polymerization to form crosslinked network. Herein, a circular disk sample of 1 mm thickness was measured using real-time FTIR coupled with UV irradiation (Fig. 2A) to understand the kinetics of photocuring process. A single layer of 1 mm thickness is simulated and the average value is calculated to compare with experimental data in order to verify the simulation results. Afterwards the simulations of layer-by-layer exposure of sliced object with mask-applied light source were conducted to study the printing process. The simulation details for kinetic study can be found in **Methods, supplementary materials**.

Firstly, various concentrations of EA samples (Table S3) were prepared by diluting with anhydrous ethanol to investigate the relationship between absorption peak value and concentration of functional group. Fig. 2B shows the FTIR spectra of 10 samples as a function of the concentration of C=C bonds in EA. With increasing concentration, the absorption peak intensity of C=C bonds increased linearly (Fig. 2C) which proved to follow Lambert–Beer behavior [22]. According to the linear least square fitting result, the concentration of C=C bonds in EA was 5.37 mol/L, which was approximating to the ideal value (5.83 mol/L) calculated with experiment data (each EA or TEMGDA molecule has difunctional C=C bonds).

Secondly, the in-situ photopolymerization experiments were carried out using FTIR spectroscopy coupled with UV irradiation to test the validity of kinetic simulations. The FTIR spectra with resolution of 4 cm^{-1} was obtained per 1.929 s in order to ensure that the UV-curing polymerization was analyzed in real time. As shown in Fig. 2D, the peak at 1628 cm^{-1} (A_{1628}) referring to the C=C stretching of the vinyl group gradually disappeared upon UV irradiation. The reaction process was traced by the degree of conversion (x) during experiment, which increased with disappearance of functional groups (C=C bonds) in FTIR absorbance, and could be calculated when a UV irradiation was given. While in simulation, the degree of conversion was calculated by the concentration change of monomer.

3.2. Physical properties

The density of EA precursor before and after cure can be determined from the linear fitting applied to the slope of accumulative total mass and volume (Fig. S2A). The EA precursor shows a similar density (1.174 g cm^{-3}) to the cured EA resin. Because EA is a typical amorphous polymer, the order of molecular chains does not change obviously compared with crystallizable thermoplastic polymers. Nevertheless, the density of EA resins decreased from 1.216 to 1.156 g cm^{-3} with the increase of concentration of PI from 1% to 3% (Fig. S2B) could have been caused by the increased dissociation rate of PI which varied the resultant crosslinked network structure. In order to study the effect of crosslinking density on the transparency of EA precursor (mixed with TPO) and cured EA resin, their absorbance at 365 nm from UV–vis spectroscopy was listed in Table S4. The coefficient of thermal expansion of EA precursor (CTE_m) and EA resins (CTE_p) was measured using a dilatometer and TMA, respectively (Figs. S2C and D), and the T_g values of EA precursor (−47.5 °C) and cured resin (83.6–85.3 °C) were summarized in Table S5. Post-curing peaks were found in UV photo-cured EA resins at ~210 °C and disappeared after being isothermal heated at 210 °C for 5 min. This phenomenon suggests that EA precursor could not be cured completely as evidenced by the fact that the conversion of C=C bond levelled off at some point.

3.3. Comparison of experiment and simulation results

Kinetic constants could be gotten according to free volume principles which free volume fractions (f_m, f_p) were calculated by the thermal expansion coefficients (α_m, α_p) and glass transition temperature (T_{gm}, T_{gp}) of the monomer and polymer.

$$f_m = 0.025 + \alpha_m(T - T_{gm}) \tag{3}$$

$$f_p = 0.025 + \alpha_p(T - T_{gp}) \tag{4}$$

The total free volume fraction f can be seen as a linear combination of f_m and f_m:

$$f = f_m\Phi_m + f_p(1 - \Phi_m) \tag{5}$$

where Φ_m is volume fraction of monomer described by the conversation of functional groups x and the density of the monomer and polymer (ρ_m, ρ_p):

$$\Phi_m = \frac{1 - x}{1 - x + \frac{\rho_m}{\rho_p}x} \tag{6}$$

Propagation (k_p) and termination (k_t) reaction kinetic constants can be calculated as follows:

$$k_p = k_{p0}\left\{1 + \exp\left[-A_p\left(\frac{1}{f} - \frac{1}{f_p}\right)\right]\right\}^{-1} \tag{7}$$

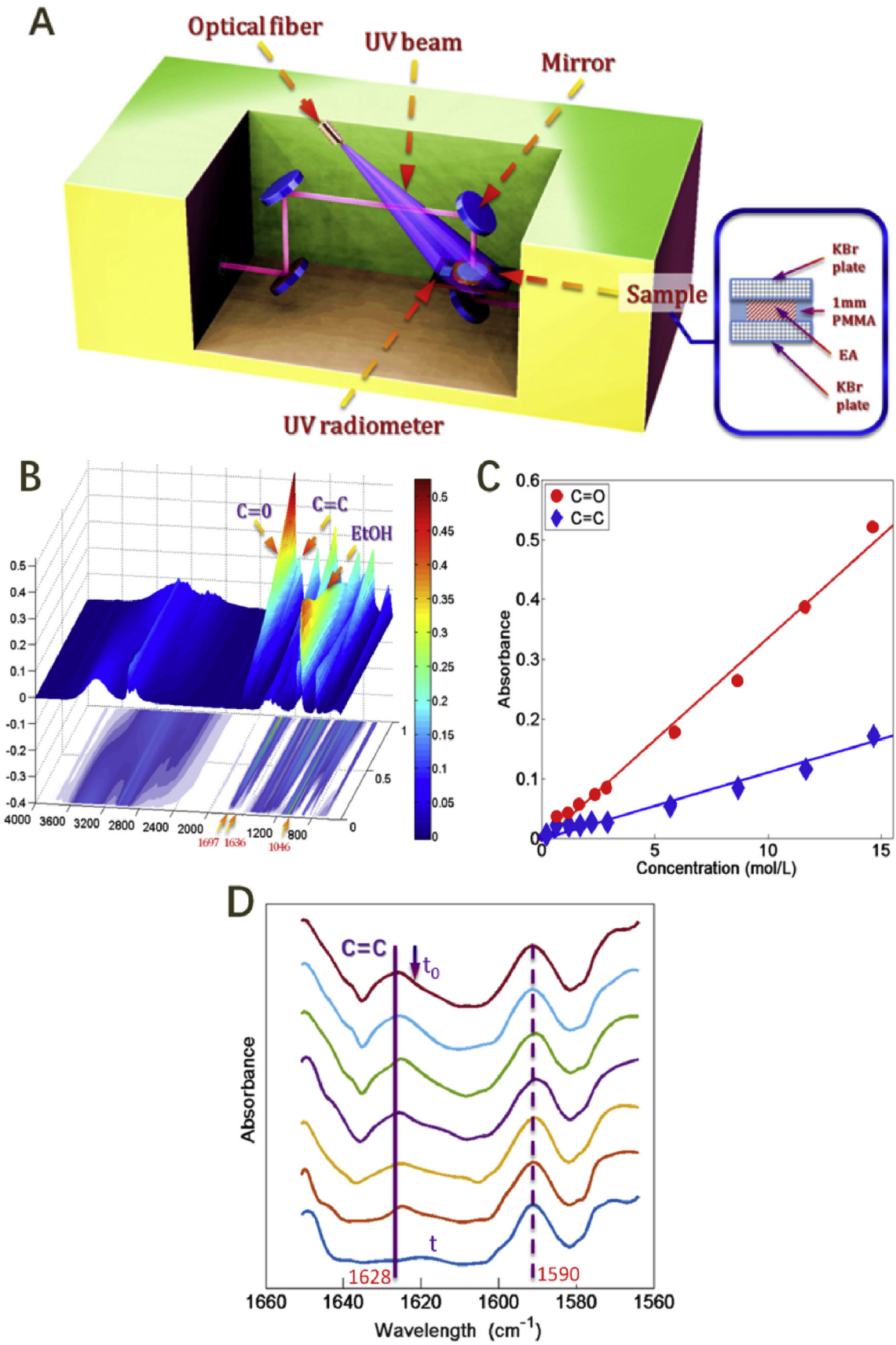

Fig. 2. The real-time FTIR measurement coupled with UV irradiation. (A) Optical setup of real-time FTIR measurement. (B) FTIR spectra of different concentration solution and (C) absorbance of function groups changing with concentration for evaluation of unknown ones. (D) FTIR absorbance of C═C function groups changing with time.

$$k_t = k_{t0}\left\{1 + \frac{1}{Rk_p\frac{[M]}{k_{t0}} + \exp\left[-A_t\left(\frac{1}{f} - \frac{1}{f_{ct}}\right)\right]}\right\}^{-1} \quad (8)$$

Light absorption could be calculated according to Beer's Law [22]. Absorption changes with initiator concentration ([PI]), and reaches constant when initiators are consumed. After gel point the absorption increases because of phase change. Initiator absorption is dependent on [PI], while background absorption depends on phase state. The system is considered liquid phase with constant background absorption (A_{0l}) before gel point, and solid phase with constant background absorption (A_{0s}) after gel point.

$$\mathrm{d}[\mathrm{I}]/\mathrm{dz} = \begin{cases}\exp(-\varepsilon[\mathrm{PI}] - A_{0l}) & x < x_g\\ \exp(-\varepsilon[\mathrm{PI}] - A_{0s}) & x \geq x_g\end{cases} \quad (9)$$

Finite element method has been applied in numerical simulation of time-dependent photocuring process shown in Fig. S1. As oxygen diffusion could be ignored, physical variables are independent with different x position. Therefore, the calculation can be carried on parallel regardless of the index order of the first dimension of the array. System.Threading.Tasks namespace in.Net framework 4.5 has been used for parallel loop. The delegate of loop function with one by-variable loop index parameter has been called in an undetermined order. Atomic operation has been applied when accessing public variables to prevent access conflict. The variables are dumped at the end of each step for analysis.

Fig. 3A shows the simulation result of photo-curing process with default parameter values for a representative sample. At the beginning of the curing process, photoinitiator molecules are excited by incident UV light and primary radicals are generated. As the reaction progresses, the viscosity is increased since radicals react with monomers and cross-linking starts to occur. As molecular mobility is reduced, termination is suppressed and autoacceleration occurs. Gelation makes the molecular mobility even lower, which leads to the propagation rate decrease after maximum rate ($R_{p,max}$). The monomer conversion at $R_{p,max}$ is considered as gel point. In our simulations we consider gel point as a constant value which is only dependent on the monomer type, regardless of initiator concentration and light intensity.

Fig. 3B shows that the reaction rate reaches the highest value ($R_{p,max}$) where t is 6.390 s, and the monomer conversion at that point is 17%, which is considered as gel point. The total square error R^2 (Eqn. (10)) was used to evaluate the experiment and simulation results of EA monomer conversion. Fig. 3C and Table S6 demonstrated that the simulation results ($Y(i)$) fit well with experimental data ($E(i)$), which verified the kinetic model for simulation.

$$\mathrm{R}^2 = 1 - \frac{1}{n}\sum_{\mathrm{i}=1}^{n}\frac{\mathrm{E(i)} - \mathrm{Y(i)}^2}{\mathrm{E(i)}} \quad (10)$$

3.4. Optimization of simulation parameters

In order to study the effect of kinetic parameters on the EA monomer conversion curve of the simulation, the reaction time of gel point (t_{gp}) and the conversion at the end of simulation (x_f) were used to reflect the curing rate and EA monomer conversion, respectively. The conversion as a function of time was simulated when the ideal propagation constant (k_{p0}) increases from 0.001 to 0.1 while other parameters remain default (Fig. 4A). Fig. 4B shows that t_{gp} is inversely proportional to k_{p0} and x_f is inversely proportional to the fourth power of k_{p0}. The curing process is faster and final conversion becomes higher as k_{p0} increases. When the ideal termination constant increases from 0.01 to 1 while other parameters remain default, t_{gp} is linear to k_{t0} and x_f is inversely proportional to k_{t0} (Fig. 4C and D), suggesting that the curing process becomes slower and final conversion becomes lower as k_{t0} increases. As the primary radical kinetic constant (k_{i0}) varies from $1e^{-6}$ to $1e^{-4}$, the x_f becomes faster and final conversion becomes higher. When the constant is too large, the conversion rate becomes slower and final conversion slightly falls down (Fig. 4E and F). As summarized up in Table S7, both k_{p0} and k_{t0} affect final conversion, and k_{i0} affects gelation speed. Higher k_{p0} or lower k_{t0} lead to higher monomer conversion, while higher k_{i0} leads to a faster curing process.

The influence of PI concentration and light intensity on the simulation results was also studied as shown in Fig. S3. The simulation curve indicates that t_{gp} increases with PI_0 in 2/3 order while x_f decreases, that is both curing speed and final conversion do not change greatly unless large concentration of PI is added. Too much PI results in low molecule weight which weakens the cured resin. It is applicable to adjust curing rate by adjusting PI concentration. When UV light intensity (I_0) is high, small changes can be observed at the conversion curve with I_0 increasing because PI dissociates much faster than propagation. The conversion process becomes much slower with decreased I_0 because of lower primary radical concentration. The effect of I_0 is similar to that of k_i, which determines curing rate but does not make a great contribution to final conversion.

The influence of layer thickness, exposure time and background absorption on printed product was investigated. In this simulation the total thickness is fixed to 2 mm while layer thickness varies from 0.1 mm to 2 mm, which means the model to be printed is sliced with different layer counts. In each simulation, the degree of conversion is lower in top layers than bottom layers. Fig. 5A shows the conversion distribution in z axis at the end of curing process. Compared to all these simulation results, a thinner layer thickness leads to higher conversion and smaller conversion difference between neighbour layers, which means a better homogeneity. Fig. 5B demonstrates the conversion curve of layer-by-layer curing with different exposure time per layer. Finer slicing causes extra time for printing process. One method is to increase exposure time without changing layer thickness. A longer exposure time leads to higher monomer conversion. To get a better printing quality, the layer below top layer should achieve a minimum conversion in order to keep the structure rigid enough for further printing, but not exceed a maximum conversion for a good interlayer connection.

The incident light is strong enough to penetrate the curing layer to cure the layers behind. When printing hanging structures, the thickness usually becomes larger as the areas behind being cured. Fig. 5C shows the simulation result of photocured resins with different concentrations of photoabsorbent that result in different background absorption. A mask is applied on the light source to simulate the shape of light beam. In real printing, the mechanical movement of platform after one layer is exposed and before the next layer exposure results in new resins flowing to the surface of printing objects. To simulate the “refreshing” process, the areas with monomer conversion lower than gel point were reset to initial concentrations of monomer, PI, oxygen, etc. after exposure of each layer. Fig. 5D shows the ratio of cured area to the area of model setting when different background absorption is applied. The printing quality is higher as photoabsorbent is added for thinner curing thickness, but too much addition result in layer separation. To obtain a better curing profile, dye or small particles could be added to reduce light penetration and light intensity or layer thickness could be programmed dependent on object geometry.

3.5. Optimize printing effect

A single layer of 2 mm thickness was monitored during 120 s curing simulation. Fig. 6A plots the depth as a function of time where liquid-gel boundary locates, which is considered cure depth. The color distribution in Fig. 6B visualized the monomer conversion. It can be seen that without addition of photoabsorbent the whole sample is cured. When the photoabsorbent is added, the cure depth is effectively limited and increases with time. To precisely control the UV light during fine structure printing, the curing depth must match the slicing thickness.

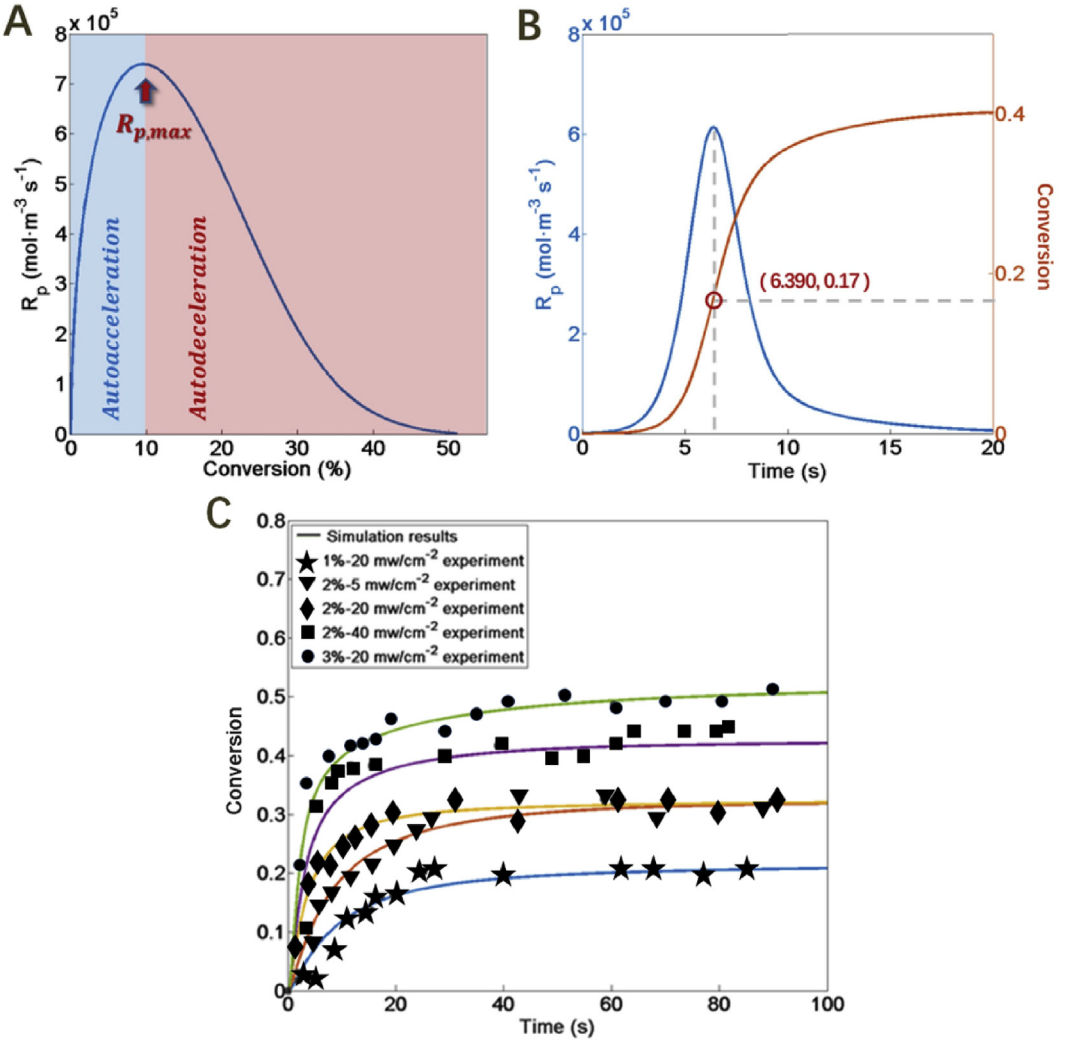

Fig. 3. The comparison of experiment data and simulation results. (A) Simulation of the photo-curing process in terms of reaction rate R_p as a function of conversion. (B) The reaction rate R_p and EA monomer conversion as a function of time. (C) The EA monomer conversion as a function of time.

Both I_0 and exposure time should be controlled in order to cure the target thickness without overexposure. With increasing I_0, the cure depth increases (Fig. 6C and D). The background absorption should be adjusted before curing by adding appropriate photoabsorbent.

Fig. 6E shows the comparison of the print preview of three different optimization strategies for the targeted object Fig. 6E(i). The printing quality of the object is shown in Fig. 6E(ii) with 5 s of time per layer and addition of photoabsorbent of $1e^4$ m^{-1}. Fig. 6E(iii) was fabricated with dynamic tunable printing time profile such as shortens the exposure time of hanging layer by 0.524 s while other layers remain the same as shown in Fig. 6E(vi). Fig. 6E(iv) showed the print preview when the light intensity was reduced to one quarter of that in Fig. 6E(ii). Fig. 6E (v) was fabricated with the additional background absorption twice of that in Fig. 6E(ii). The above three approaches effectively improved the overexposure which resulted in a thicker shell as shown in Fig. 6E(ii) and well matches the expected geometry. In practice, resin and printing parameters should be optimized at the same time to improve print resolution without slowing down the printing speed.

4. Discussions

The central aim of this work is the simulation of photopolymerization for SL 3D printing to realize visualization of printing quality before practically printing the targeted objects with complex topology structures or expensive materials, that we named 3D printing preview. Following a bottom-up approach, in this work, we focused on a general UV-curable EA resin and SL 3D printing apparatus. Complete kinetic models for this representative example have been developed to describe photopolymerization process including diffusion of monomers, radicals and oxygen, propagation and termination. From microscopical aspects, thickness and exposure time of layers, light density of light resource and post-curing time are curial parameters needed to consider in the 3D printing process of complex structure to get an ideal product in as little time as possible [23]. In microcosmic aspects, the photopolymerization behavior such as the polymerization rate and conversion of functional groups, etc. depends on monomer structure and reaction conditions which can lead to products with widely differing characteristics [24]. Thus, our simulations show that high quality 3D printing result can be obtained with the dynamic adjustment of parameters such as light intensity, exposure time, and weight percent UV absorber, etc.

UV-curable resins (Table S8) are generally divided into two classes depending on whether the reaction proceeds by a radical-type or cationic-type mechanism [25]. Discrete techniques include infrared, photoacoustic, nuclear magnetic resonance spectroscopy, etc. which measure states of monomers reaction halted at some time until reaction ended, while continuous methods used in common include calorimetry [26], rheometer [27], FT-IR and UV/vis [28], etc. to monitor the in-situ reactions. Therefore, an exclusive database for 3D printing with

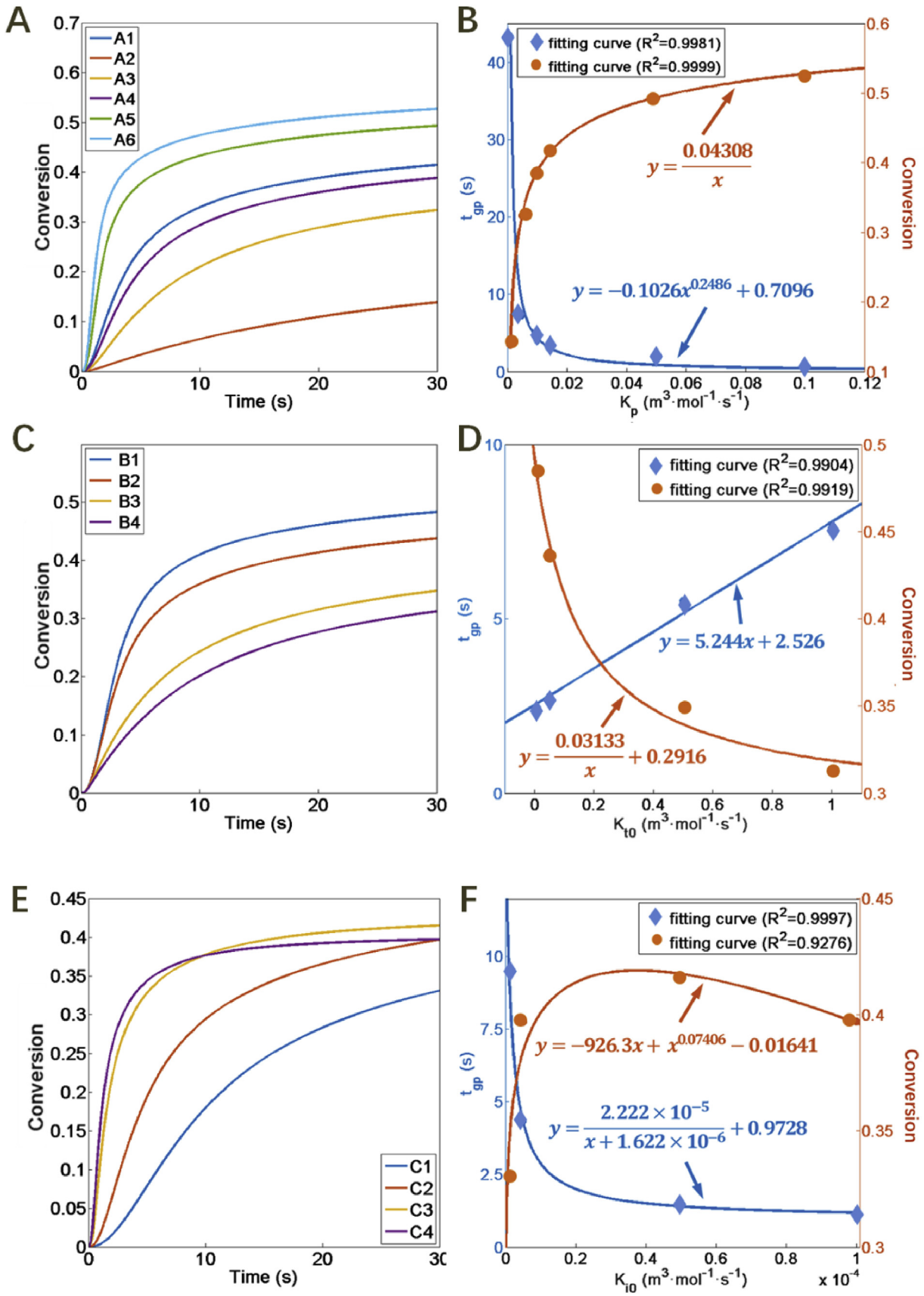

Fig. 4. Simulation results for the effect of k_{p0}, k_{t0}, and k_{i0} on curing process. (A) The values of k_{p0} were set to be: A1 = 0.1, A2 = 0.05, A3 = 0.014, A4 = 0.01, A5 = 0.005, and A6 = 0.001, respectively. (B) The gel point (t_{gp}) and end of conversion (x_f) as a function of k_{p0} ranging from 0.001 to 0.1. (C) The values of k_{t0} were set to be: B1 = 0.5, B2 = 0.1, B3 = 0.05, and B4 = 0.01, respectively. (D) t_{gp} and x_f as a function of k_{t0} ranging from 0.01 to 1. (E) The values of k_{i0} were set to be: C1 = $1e^{-4}$, C2 = $5e^{-5}$, C3 = $5e^{-6}$, and C4 = $1e^{-6}$, respectively. (F) t_{gp} and x_f as a function of k_{i0} ranging from $1e^{-6}$ to $1e^{-4}$. The unit of k_{p0}, k_{t0}, and k_{i0} is m [3] $\cdot mol^{-1} \cdot s^{-1}$.

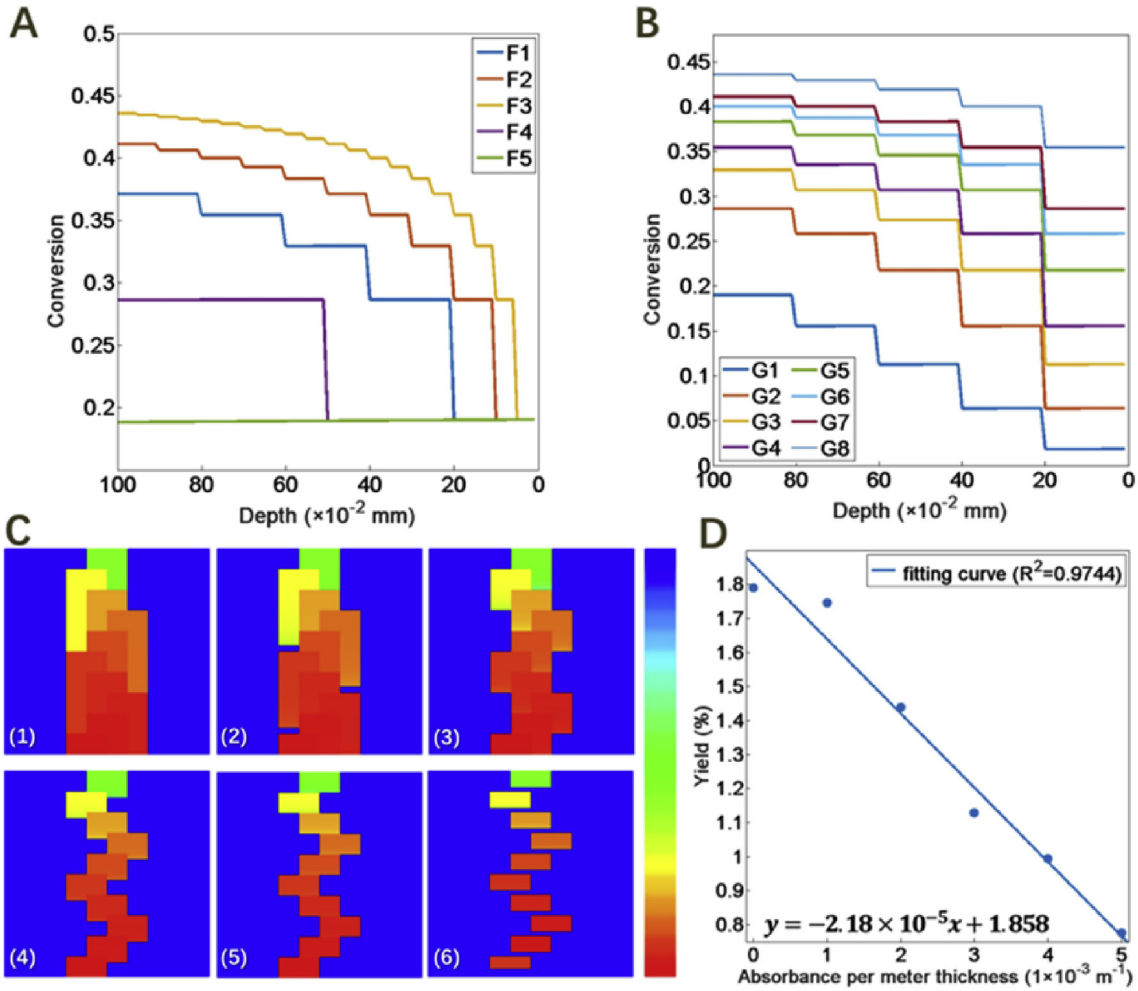

Fig. 5. Simulation results for the effect of layer thickness, exposure time and photoabsorbent on printing quality. (A) The layer thickness was set to be: F1 = 0.2 mm, F2 = 0.1 mm, F3 = 0.05 mm, F4 = 0.5 mm, and F5 = 1 mm, respectively. (B) The exposure time of each layer was set to be: G1 = 1 s, G2 = 2 s, G3 = 3 s, G4 = 4 s, G5 = 6 s, G6 = 8 s, G7 = 10 s, and G8 = 20 s, respectively. (C) The background absorption constant for photoabsorbent as (1) 0 m^{-1}, (2) $1e^4$ m^{-1}, (3) $2e^4$ m^{-1}, (4) $3e^4$ m^{-1}, (5) $4e^4$ m^{-1} and (6) $5e^4$ m^{-1}, respectively. (D) Ratio of cured area to model area.

massive UV-curable resins can be established based on the simulations of the monomers from forming crosslinked network to printed products. This could place SL 3D printing technology beyond the research laboratories and prototype development niche to become more economically viable alternative to additive manufacturing.

5. Conclusions

In summary, different formulations of dental materials based on EA precursor and TPO as photoinitiator were used as representative example to show how to use the photopolymerization kinetic models to realize SL 3D printing preview. We combined the layer-to-layer mechanism and crosslinking reaction with oxygen inhibition kinetic models to predict printing effects with different settings schemes. And this model is applicable for any light source in theory. For more realistic simulations of different resins, apart from default settings, several kinetic curves could be measured by in-situ FTIR for the program to calculate a set of corresponding kinetics parameters as input data source. Results showed that printing settings really had a great influence on printing quality for paradoxical relationship between print speed and resolution and proper dynamic time control would not only improve print resolution but also decline time consuming. Therefore, a print preview strategy of program controllable time- and thickness-varying was successfully realized.

CRediT authorship contribution statement

Yi Gao: Methodology, Investigation, Writing - original draft. **Lei Xu:** Investigation, Writing - original draft. **Yang Zhao:** Investigation. **Zhengwei You:** Supervision, Writing - review & editing. **Qingbao Guan:** Supervision, Conceptualization, Resources, Writing - original draft, Writing - review & editing.

Declaration of competing interest

The authors declare no conflict of interest.

Acknowledgment

This work was supported by the National Natural Science Foundation of China (51703148, 21574019), China; China Postdoctoral Science Foundation (2017M611901), China; Fundamental Research Funds for the Central Universities (2232019D3-07), China; Shanghai Belt and Road Joint Laboratory of Advanced Fiber and Low-dimension Materials (18520750400), China; Key Laboratory of High-Performance Fibers & Products, Ministry of Education, Center for Civil Aviation Composites, Donghua University and Key Laboratory of Shanghai City for Lightweight Composites (X12811901/018), China; and Initial Research Funds for Young Teachers of Donghua University, China.

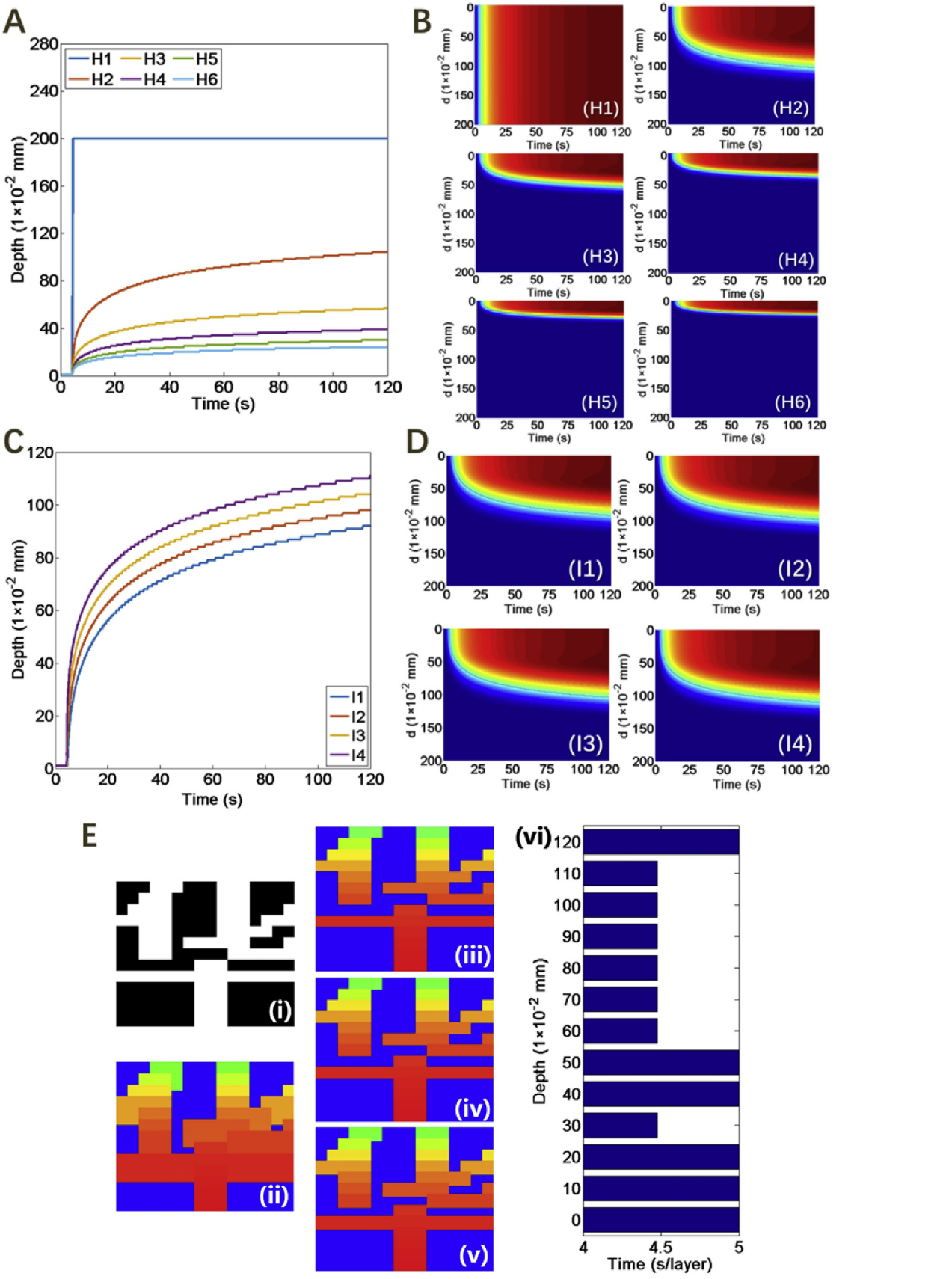

(caption on next page)

Fig. 6. Simulation results for the effect of cure depth and photoabsorbent on print preview. (A) The addition of photoabsorbent as a function of cure depth and (B) their distribution diagram. The background absorption constant for photoabsorbent was set to be: H1 = 0 m^{-1}, H2 = $1e^4$ m^{-1}, H3 = $2e^4$ m^{-1}, H4 = $3e^4$ m^{-1}, H5 = $4e^4$ m^{-1}, and H6 = $5e^4$ m^{-1}, respectively. (C) The cure depth with different I_0 values as a function of time and (D) their distribution diagram. I_0 values were set to be: I1 = 5, I2 = 10, I3 = 20, and I4 = 40, respectively. The unit of I_0 is mw·m^2. (E) The print preview compares different optimization strategies. (i) Targeted printing pattern, a Chinese character "Hua"; (ii) The preview with equal exposure time (5 s) per layer; (iii) The preview with dynamic tunable exposure time compared with (ii); (iv) The preview with one quarter light intensity compare with (ii); (v) The preview with twice background absorbance as much as that in (ii); (vi) Detailed tunable exposure time for each layer in (iii).

Appendix A. Supplementary data

Supplementary data to this article can be found online at https://doi.org/10.1016/j.bioactmat.2020.05.006.

References

[1] I.D. Robertson, M. Yourdkhani, P.J. Centellas, J.E. Aw, D.G. Ivanoff, E. Goli, E.M. Lloyd, L.M. Dean, N.R. Sottos, P.H. Geubelle, J.S. Moore, S.R. White, Rapid energy-efficient manufacturing of polymers and composites via frontal polymerization, Nature 557 (2018) 223–227.

[2] Z. Lin, M. Wu, H. He, Qi Liang, C. Hu, Z. Zeng, D. Cheng, G. Wang, D. Chen, H. Pan, C. Ruan, 3D printing of mechanically stable calcium-free alginate-based scaffolds with tunable surface charge to enable cell adhesion and facile biofunctionalization, Adv. Funct. Mater. 29 (2019) 1808439–1808452.

[3] J.R. Tumbleston, D. Shirvanyants, N. Ermoshkin, R. Janusziewicz, A.R. Johnson, D. Kelly, K. Chen, R. Pinschmidt, J.P. Rolland, A. Ermoshkin, E.T. Samulski, J.M. DeSimone, Additive manufacturing. Continuous liquid interface production of 3D objects, Science 347 (2015) 1349–1352.

[4] C. Wang, W. Huang, Y. Zhou, L. He, Z. He, Z. Chen, X. He, S. Tian, J. Liao, B. Lua, Y. Wei, M. Wang, 3D printing of bone tissue engineering scaffolds, Bioact. Mater. 5 (2020) 82–91.

[5] J.W. Stansbury, M.J. Idacavage, 3D printing with polymers: challenges among expanding options and opportunities, Dent. Mater. 32 (2016) 54–64.

[6] E. Andrzejewska, Photopolymerization kinetics of multifunctional monomers, Prog. Polym. Sci. 26 (2001) 605–665.

[7] N. Guo, M.C. Leu, Additive manufacturing: technology, applications and research needs, Front. Mech. Eng.-Prc. 8 (2013) 215–243.

[8] P. Mohan Pandey, N. Venkata Reddy, S.G. Dhande, Slicing procedures in layered manufacturing: a review, Rapid Prototyp. J. 9 (2003) 274–288.

[9] S.C. Ligon, R. Liska, J. Stampfl, M. Gurr, R. Mulhaupt, Polymers for 3D printing and customized additive manufacturing, Chem. Rev. 117 (2017) 10212–10290.

[10] S.C. Ligon, B. Husar, H. Wutzel, R. Holman, R. Liska, Strategies to reduce oxygen inhibition in photoinduced polymerization, Chem. Rev. 114 (2014) 557–589.

[11] R. Janusziewicz, J.R. Tumbleston, A.L. Quintanilla, S.J. Mecham, J.M. DeSimone, Layerless fabrication with continuous liquid interface production, Proc. Natl. Acad. Sci. U.S.A. 113 (2016) 11703–11708.

[12] Z. Wang, H. Liang, A.V. Dobrynin, Computer simulations of continuous 3D printing, Macromolecules 50 (2017) 7794–7800.

[13] Y. Zhang, D.E. Kranbuehl, H. Sautereau, G. Seytre, J. Dupuy, Study of UV cure kinetics resulting from a changing concentration of mobile and trapped radicals, Macromolecules 41 (2008) 708–715.

[14] Y. Zhang, D.E. Kranbuehl, H. Sautereau, G. Seytre, J. Dupuy, Modeling and measuring UV cure kinetics of thick dimethacrylate samples, Macromolecules 42 (2009) 203–210.

[15] R. Anastasio, W. Peerbooms, R. Cardinaels, L.C.A. van Breemen, Characterization of ultraviolet-cured methacrylate networks: from photopolymerization to ultimate mechanical properties, Macromolecules 52 (2019) 9220–9231.

[16] J.P. Kruth, M.C. Leu, T. Nakagawa, Progress in additive manufacturing and rapid prototyping, CIRP Annals 47 (1998) 525–540.

[17] G. Kumaraswamy, Thermodynamics of high polymer solutions, Resonance 22 (2017) 415–426.

[18] C. Decker, K. Moussa, Real-time kinetic study of laser-induced polymerization, Macromolecules 22 (1989) 4455–4462.

[19] P. Liu, A. Gu, G. Liang, Q. Guan, L. Yuan, Preparation and properties of novel high performance UV-curable epoxy acrylate/hyperbranched polysiloxane coatings, Prog. Org. Coating 74 (2012) 142–150.

[20] J. Christmann, C. Ley, X. Allonas, A. Ibrahim, C. Croutxé-Barghorn, Experimental and theoretical investigations of free radical photopolymerization: inhibition and termination reactions, Polymer 160 (2019) 254–264.

[21] S.C. Ligon-Auer, M. Schwentenwein, C. Gorsche, J. Stampfl, R. Liska, Toughening of photo-curable polymer networks: a review, Polym. Chem. 7 (2016) 257–286.

[22] Y. Hernandez, V. Nicolosi, M. Lotya, F.M. Blighe, Z. Sun, S. De, I.T. McGovern, B. Holland, M. Byrne, Y.K. Gun'Ko, J.J. Boland, P. Niraj, G. Duesberg, S. Krishnamurthy, R. Goodhue, J. Hutchison, V. Scardaci, A.C. Ferrari, J.N. Coleman, High-yield production of graphene by liquid-phase exfoliation of graphite, Nat. Nanotechnol. 3 (2008) 563–568.

[23] Y. Yagci, S. Jockusch, N.J. Turro, Photoinitiated polymerization: advances, challenges, and opportunities, Macromolecules 43 (2010) 6245–6260.

[24] T. Vidil, F. Tournilhac, S. Musso, A. Robisson, L. Leibler, Control of reactions and network structures of epoxy thermosets, Prog. Polym. Sci. 62 (2016) 126–179.

[25] C. Decker, Kinetic study and new applications of uv radiation curing, Macromol. Rapid Commun. 23 (2002) 1067–1093.

[26] W.-S. Kim, K.-S. Park, J.H. Nam, D. Shin, S. Jang, T.-Y. Chung, Fast cure kinetics of a UV-curable resin for UV nano-imprint lithography: phenomenological model determination based on differential photocalorimetry results, Thermochim. Acta 498 (2010) 117–123.

[27] B.-S. Chiou, S.R. Raghavan, S.A. Khan, Effect of colloidal fillers on the cross-linking of a UV-curable polymer: gel point rheology and the winter – chambon criterion, Macromolecules 34 (2001) 4526–4533.

[28] A. Aguirre-Soto, A.T. Hwang, D. Glugla, J.W. Wydra, R.R. McLeod, C.N. Bowman, J.W. Stansbury, Coupled UV–Vis/FT–NIR spectroscopy for kinetic analysis of multiple reaction steps in polymerizations, Macromolecules 48 (2015) 6781–6790.